INSTITUTE OF PHYSICS PUBLISHING MODELLING AND SIMULATION IN MATERIALS SCIENCE AND ENGINEERING

Modelling Simul. Mater. Sci. Eng. **14** (2006) 1139–1151 doi:10.1088/0965-0393/14/7/003

A hybrid method for computing forces on curved dislocations intersecting free surfaces in three-dimensional dislocation dynamics

Meijie Tang[1], Wei Cai[2], Guanshui Xu[3] and Vasily V Bulatov[1]

[1] Lawrence Livermore National Laboratory, Livermore, CA 94551, USA
[2] Mechanical Engineering Department, Stanford University, Stanford, CA 94305, USA
[3] Mechanical Engineering Department, University of California, Riverside, CA 92521, USA

E-mail: tang7@llnl.gov

Received 1 February 2006, in final form 21 June 2006
Published 21 August 2006
Online at stacks.iop.org/MSMSE/14/1139

Abstract

Dislocations intersecting free surfaces present a challenge for numerical implementation of traction-free boundary conditions in dislocation dynamics simulations. The difficulty arises when singular analytic expressions of dislocation stress fields need to be used in combination with numerical methods to calculate image stress fields due to the free surfaces. A new hybrid method is developed here in which the singular and non-singular parts of the image stress are dealt with separately. The analytic solution for a semi-infinite straight dislocation intersecting the surface of elastic half-space is used to account for the singular part of the image stress, while the remaining non-singular part is treated using the standard finite element method. The numerical advantages of this decomposition are demonstrated with examples.

(Some figures in this article are in colour only in the electronic version)

1. Introduction

During the last decade dislocation dynamics (DD) simulations have emerged as a useful numerical approach for studying the mechanical behaviour of crystals based on the fundamental mechanisms of dislocation motion (Kubin and Canova 1992, Tang *et al* 1998, Zbib *et al* 1998, Ghoniem *et al* 2000, Schwarz 1999). For example, direct simulation of dislocation behaviour in thin films and microelectronic devices is an appealing application of this relatively new approach (Schwarz 1999, Wang *et al* 2004). General aspects of the DD method have been extensively reviewed in the literature (Bulatov *et al* 2001, Weygand *et al* 2002, Devincre 1996). Briefly speaking, the DD simulations track the motion of dislocation lines, which are usually represented by a set of inter-connected segments. The dislocations move in response to forces that are proportional to the local stress field generated by external loads, other dislocations or

other types of defects, such as cracks. For a bulk single crystal, the major computational time of DD simulations is spent on the evaluation of the stress field produced by the dislocation segments themselves. These simulations use the analytic expressions for the dislocation stress field in an infinite elastic medium (Hirth and Lothe 1982, Devincre 1995), which will be referred to as the canonical solutions of dislocations in the following discussions.

When the canonical solutions are applied to a finite elastic body, traction forces exist on the boundary surfaces. These traction forces should then be removed if the elastic body is subjected to traction-free boundary conditions. The image stress is defined as the additional stress field due to such a correction; the total stress field is the summation of the canonical and image stress fields. This two-step approach to obtain dislocation stress fields that satisfy traction-free surface boundary conditions has a long history in the literature (Eshelby 1979, Van der Giessen and Needleman 1995, Fivel *et al* 1996, Yasin *et al* 2001, Lemchand *et al* 2001). Boundary element method (BEM) and finite element method (FEM) are two standard numerical methods to compute the image stress, given the spurious traction forces that need to be cancelled. Both BEM (Fivel *et al* 1996, Liu *et al* 2000) and FEM (Martinez and Ghoniem 2002, Tang *et al* 2003) have been implemented in DD simulations of a finite elastic body.

This approach works well when all dislocation segments are sufficiently away from the free surface, so that the spurious surface traction forces are slowly varying functions. Unfortunately, this approach becomes very inefficient when one or more dislocation segments intersect the surface. Because the canonical stress field is singular on the dislocation line, the spurious surface tractions are singular at the intersection point. When standard FEM is applied to solve for the image stress due to such singular traction forces, the result is found to strongly depend on the mesh size (Tang *et al* 2003). In principle, the numerical values for the forces on dislocation segments should eventually converge if the mesh is made fine enough. However, the numerical convergence is found to be very slow (for test cases whose exact solutions are available for comparison). When a uniform mesh is used, the total number of mesh points often becomes impractically large before numerical convergence is reached. Other difficulties arise when threading dislocations move and overlap with the Gaussian integration points of the FEM mesh, leading to numerical instabilities. A possible solution is to use adaptive meshes with multiple resolutions that follow the intersection points (Liu and Schwarz 2005). But adaptive meshing is a cumbersome and challenging problem in itself, especially for large scale DD simulations where many dislocations intersect the surface. To speed up the numerical convergence of image stress calculation, Weygand *et al* (2002) attempted to make the spurious surface tractions vary as slowly as possible, by adjusting 'virtual' dislocation segments, such as by the 'mirror-image' construction. Unfortunately, the 'virtual' dislocation segments do not completely remove the singularity from the spurious surface traction. Hence the FEM calculation still faces the same type of problems associated with the singularity. It is worth mentioning that a different approach using prismatic loops on the free surfaces to account for the image stress without utilizing FEM was developed for DD simulation (Khraishi and Zbib 2002, Yan *et al* 2004). However, this method is computationally very expensive.

In this paper, we describe an alternative approach to speed up the numerical convergence of the image stress calculation. In this approach, the singularity is completely removed from the FEM calculation, which now converges significantly faster than before and a much coarser mesh can be used. The idea is to consider the image stress field as the superposition of two solutions. The first solution is the image stress field of a semi-infinite straight dislocation intersecting the free surface of a half-space, for which analytic expressions exist. The geometry of this (auxiliary) straight dislocation is chosen such that its image stress contains the same singularity as the image stress of the dislocation of interest. The second solution is the difference between these two image stress fields; by construction it is a non-singular function of space and is

solved numerically, such as by FEM. Hence the image stress of interest is obtained as the hybrid of analytic and FEM solutions. Even though the analytic solution used here exists in an elastic subspace, our hybrid approach can be generalized to a finite elastic body with multiple free surfaces. The key difference between the present and previous approaches is that the singularity is completely removed from our numerical calculation, which fundamentally changes the nature of the problem that FEM needs to deal with.

In the next section, we give a brief overview of the DD and FEM models used in this work. The new hybrid method is presented in section 3 and some examples are discussed in section 4. Finally, some conclusive remarks are made in section 5.

2. Methodology

2.1. Dislocation dynamics

In our DD model, the dislocation lines are represented by straight segments connecting a set of nodes. The nodal position $\boldsymbol{r}_\mathrm{i}$ and the Burgers vectors of the segments $\boldsymbol{b}_\mathrm{ij}$ (i and j refer to the two ending nodes of the segment) are the degrees of freedom in this model (Cai *et al* 2004b, Bulatov *et al* 2004). The driving force $\boldsymbol{f}_\mathrm{i}$ on every node is computed at the beginning of every time step. It is the weighted average of the Peach-Koehler (PK) forces acting on the dislocation segments connected to the node (Cai 2001, Kukta 1998 , Weygand *et al* 2002), i.e.

$$\boldsymbol{f}_\mathrm{i} = \int_\mathrm{C} \boldsymbol{f}^{\,\mathrm{PK}}(\boldsymbol{x})\mathrm{N_i}(\boldsymbol{x})\mathrm{dL}(\boldsymbol{x}), \tag{1}$$

where the integral is along all segments connected to node i. $\mathrm{N_i}(\boldsymbol{x})$ is a shape function that equals to one at node i and decreases linearly to zero at neighbouring nodes. The PK force per unit length on a dislocation segment at point $\boldsymbol{x}$ is

$$\boldsymbol{f}^{\,\mathrm{PK}}(\boldsymbol{x}) = (\boldsymbol{\sigma}(\boldsymbol{x}) \cdot \boldsymbol{b}) \times \boldsymbol{\xi}(\boldsymbol{x}), \tag{2}$$

where $\boldsymbol{\sigma}(\boldsymbol{x})$ and $\boldsymbol{\xi}(\boldsymbol{x})$ are the stress tensor and the unit tangent vector at point $\boldsymbol{x}$ on the segment and $\boldsymbol{b}$ is its Burgers vector. The stress field $\boldsymbol{\sigma}(\boldsymbol{x})$ is the sum of applied stress and internal stress field produced by all dislocation segments in the model. In isotropic elasticity, analytic expressions are available for the stress field produced by an arbitrary straight dislocation in an infinite elastic medium (Hirth and Lothe 1982). In a finite elastic medium,$\boldsymbol{\sigma}(\boldsymbol{x})$should have several contributions, i.e. $\boldsymbol{\sigma}(\boldsymbol{x}) = \boldsymbol{\sigma}^{\mathrm{app}}(\boldsymbol{x}) + \boldsymbol{\sigma}^{\infty}(\boldsymbol{x}) + \boldsymbol{\sigma}^{\mathrm{img}}(\boldsymbol{x})$. The first term $\boldsymbol{\sigma}^{\mathrm{app}}(\boldsymbol{x})$ is the applied stress, the second term $\boldsymbol{\sigma}^{\infty}(\boldsymbol{x})$ is the internal stress field due to all the dislocations in the system and the third term $\boldsymbol{\sigma}^{\mathrm{img}}(\boldsymbol{x})$ is the image stress due to the free surfaces. In this paper, no applied stress is present.

Because the dislocation stress field is singular on the dislocation lines themselves, some truncation has to be applied to avoid this singularity. In this study, we adopt a simple approach proposed by Brown (1964), in which the stress field is never computed on the segment itself. Instead, stress is computed first on both sides of the segment on the glide plane at a distance ρ to the segment and then the average of the two stress values is used for computing the PK force $\boldsymbol{f}^{\,\mathrm{PK}}(\boldsymbol{x})$ (Schwarz 1999). There are several limitations to Brown's approach. For example, one needs to specify a plane on which the two stress evaluating points are located, which may be ad hoc for screw dislocations or non-screw dislocations undergoing climb. Brown's approach was also shown to lack self-consistency (Gavazza and Barnett 1976) and alternative approaches have been proposed (Lothe 1992, Cai *et al* 2005). Because the focus of this paper is on image stress calculation, we adopt Brown's approach for simplicity and constrain all dislocation segments to a pre-specified glide plane.

Following nodal force is the calculation of nodal velocities. In most cases of interest, the effect of inertia on dislocation motion can be ignored so that the equation of motion is first-order, i.e. the driving forces determine the instantaneous velocities through a mobility function (Cai and Bulatov 2004, Cai *et al* 2004a). For simplicity, we use a linear mobility function

$$\boldsymbol{v}_{\mathrm{i}} = \mathrm{M}\mathrm{g}_{\mathrm{i}}\mathrm{H}(\mathrm{g}_{\mathrm{i}})\boldsymbol{t}_{\mathrm{i}}, \tag{3}$$

$$\boldsymbol{t}_{\mathrm{i}} = \boldsymbol{f}_{\mathrm{i}} / \left|\boldsymbol{f}_{\mathrm{i}}\right|, \tag{4}$$

$$\mathrm{g}_{\mathrm{i}} = \left|\boldsymbol{f}_{\mathrm{i}}\right| / \mathrm{L}_{\mathrm{i}} - \tau_{\mathrm{p}}\mathrm{b}, \tag{5}$$

where $\boldsymbol{v}_{\mathrm{i}}$ is the velocity of node i, $\boldsymbol{t}_{\mathrm{i}}$ is the unit vector along $\boldsymbol{f}_{\mathrm{i}}$, M is a mobility constant, and L_{i} is half of the total length of all segments connected to node i, τ_{p} is the minimal stress required for dislocation motion (i.e. Peierls stress) and b is the magnitude of the Burgers vector. H(x) is a step function that equals one if $x > 0$ and equals zero if $x < 0$. The step function guarantees that the velocity is zero when the driving force per unit length is smaller than the resistance force due to the Peierls stress. Notice that here $\boldsymbol{v}_{\mathrm{i}}$, $\boldsymbol{t}_{\mathrm{i}}$ and $\boldsymbol{f}_{\mathrm{i}}$ are all two-dimensional vectors on the glide plane. The Burgers vectors remain unchanged during nodal motion, unless dislocation reaction occurs, such as when two dislocation segments combine into one. In this case a new segment appears with the Burgers vector being the sum of the two original Burgers vectors.

2.2. Finite element method

The FEM is a standard approach to solve boundary value problems in elasticity (Hughes 2000, Smith and Griffiths 1998). In this case, it is used to solve for the image stress field due to the surface tractions for correcting the canonical stress field. The FEM code used in this work relies on direct and conjugate gradient iterative solvers. The latter is considerably more efficient for large systems with thousands of elements or more. Regular meshes (i.e. 8-node linear cubic brick elements) are used throughout this study with the mesh size ranging from 0.1 to 0.6 nm. The largest system reported here contains 10.8 million elements. For simplicity, the stress field is sampled at one Gaussian point in each element. This means that the stress at any point in space is taken as the stress value in the element that contains this point. We have also implemented a scheme in which the stress at a given field point is interpolated based on the stress values of the nearest 8 Gaussian points around the field point. This does not change the general conclusion of this paper.

All the calculations discussed here use rectangular simulation boxes with larger x and y dimensions and a smaller z dimension. For the cases with only one free surface at the top (with z axis as the normal direction), zero-displacement boundary conditions were applied to all the other five surfaces unless otherwise noted. For the cases with two free surfaces, one at the top and the other at the bottom, the zero-displacement boundary conditions were applied to the four side surfaces.

3. The hybrid method for image stress calculation

Consider the case of a curved dislocation, discretized into a set of straight segments, intersecting the free surface of an elastic half-space, as shown in figure 1(*a*). Our task is to find the stress field $\boldsymbol{\sigma}(\boldsymbol{x})$ inside the elastic medium, so that we can evaluate the forces on the dislocation segments for DD simulations. This is usually done by first imagining that the dislocation actually exists in an infinite elastic medium. For this purpose we also need to continue the dislocation beyond node 0 to infinity, usually as a straight line, so that the dislocation does

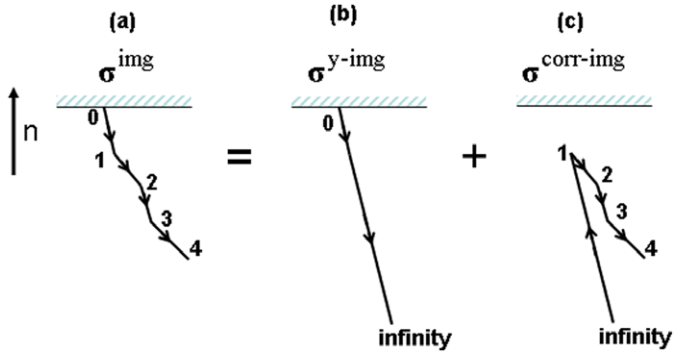

Figure 1. Decomposition and superposition used to formulate the hybrid method are illustrated schematically for a half-space with only one free surface. As a source of stress, an arbitrarily shaped dislocation (*a*) terminating at the free surface is viewed here as a sum of two configurations, i.e. (*b*) and (*c*). The Yoffe solution applies directly to (*b*) and the standard FEM is used to calculate the image stress for (*c*).

not end inside the elastic medium. Let the corresponding stress field be $\boldsymbol{\sigma}^{\infty}(\boldsymbol{x})$. The traction force on the boundary surface is $\boldsymbol{F}(\boldsymbol{x}) = \boldsymbol{\sigma}^{\infty}(\boldsymbol{x}) \cdot \boldsymbol{n}$, where $\boldsymbol{n}$ is the surface normal vector. If we wish to apply a traction-free boundary condition to the surface instead, we will need to find the image stress $\boldsymbol{\sigma}^{\mathrm{img}}(\boldsymbol{x})$ generated in the elastic half-space, with the traction force boundary condition as $\boldsymbol{T}(\boldsymbol{x}) = -\boldsymbol{\sigma}^{\infty}(\boldsymbol{x}) \cdot \boldsymbol{n}$ applied to its surface. The total stress is the sum of the two: $\boldsymbol{\sigma}(\boldsymbol{x}) = \boldsymbol{\sigma}^{\infty}(\boldsymbol{x}) + \boldsymbol{\sigma}^{\mathrm{img}}(\boldsymbol{x})$. As stated above, given $\boldsymbol{T}(\boldsymbol{x})$, the difficulty of solving for $\boldsymbol{\sigma}^{\mathrm{img}}(\boldsymbol{x})$ numerically is that $\boldsymbol{T}(\boldsymbol{x})$ is singular at the point where the dislocation intersects the surface. Consequently, $\boldsymbol{\sigma}^{\mathrm{img}}(\boldsymbol{x})$ is also singular at this point.

However, if the dislocation is perfectly straight, as shown in figure 1(*b*), then we do not need to solve this problem numerically. Analytical expressions have been derived by Yoffe (1961), with several misprints later on corrected by Shaibani and Hazzledine (1981) and Hazzledine and Shaibani (1982). In the following, we will refer to the total and image stress for this configuration as $\boldsymbol{\sigma}^{y}(\boldsymbol{x})$ and $\boldsymbol{\sigma}^{y-\mathrm{img}}(\boldsymbol{x})$, respectively.

Let us return to the problem of solving for the image stress $\boldsymbol{\sigma}^{\mathrm{img}}(\boldsymbol{x})$ in figure 1(*a*). We notice that the difference between $\boldsymbol{\sigma}^{\mathrm{img}}(\boldsymbol{x})$ and $\boldsymbol{\sigma}^{y-\mathrm{img}}(\boldsymbol{x})$ is exactly the image stress of a different dislocation, shown in figure 1(*c*), which does not intersect the surface. Let us call the image stress of this dislocation $\boldsymbol{\sigma}^{\mathrm{corr}-\mathrm{img}}(\boldsymbol{x})$. The image stress in figure 1(*a*) can be obtained as $\boldsymbol{\sigma}^{\mathrm{img}}(\boldsymbol{x}) = \boldsymbol{\sigma}^{y-\mathrm{img}}(\boldsymbol{x}) + \boldsymbol{\sigma}^{\mathrm{corr}-\mathrm{img}}(\boldsymbol{x})$, where $\boldsymbol{\sigma}^{y-\mathrm{img}}(\boldsymbol{x})$ is available in analytic form and $\boldsymbol{\sigma}^{\mathrm{corr}-\mathrm{img}}(\boldsymbol{x})$ can be computed numerically such as by FEM. The important point is that, in this approach, FEM does not need to deal with a singular surface traction any more. Hence the numerical convergence is much faster and a much coarser mesh can be used than before. In the following, we describe some benchmark results and further generalizations of this idea.

3.1. Validation of Yoffe solution implementation

First, we validate our numerical implementation of the Yoffe image stress solution, by comparing it with a direct FEM calculation. The FEM calculation deals with a rectangular solid with x, y and z dimensions at 60 nm, 60 nm and 6 nm, respectively. The top surface at $z = 6$ nm is subjected to free-surface boundary condition. The Burgers vector is along the [111] direction and its magnitude is 0.286 nm. The dislocation line is at 5° with the z-axis (i.e.

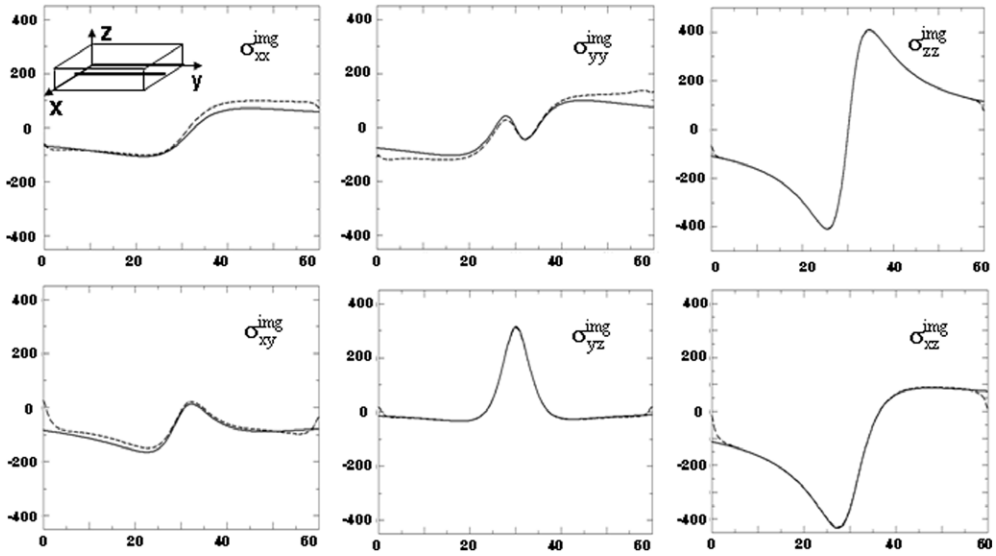

Figure 2. Six components of the image stress tensor as a function of y beneath the surface of an elastic half-space, for a straight semi-infinite mixed dislocation intersecting the surface at 5° to the surface normal. Stresses are in units of MPa and length is in units of nm. The solid lines are for the Yoffe solution and the dashed lines are for the direct FEM calculation. The inset in top left panel shows the position of the line along which the stress values are shown.

[001] direction). The FEM mesh is formed by cubes of 0.2 nm in length. The Yoffe image stress solution and the image stress obtained by direct FEM are compared along a line parallel to the y axis at $x = 30$ nm and $z = 0.6$ nm (see the inset in figure 2). The six stress components from the two approaches are plotted in figure 2.

In the FEM calculation, only the top surface is assumed to be free of traction. Zero displacement boundary conditions are applied at four side surfaces. To minimize possible artefacts, a fixed surface traction boundary condition is used at the bottom surface with the tractions computed from the Yoffe total stress analytic solution. This was found to have a better agreement with the Yoffe image stress solution for the stress field close to the bottom surface. As shown in figure 2, the FEM results agree well with the Yoffe analytic solution except close to the side surfaces, which is an artefact of the zero-displacement boundary condition used in the FEM calculation. As an additional test for consistency, we verified that, when a dislocation is perpendicular to the free surface, the stress field reduces analytically from the general Yoffe solution to the one found by Honda (1979).

3.2. Comparison between hybrid and direct FEM approaches

A simple test to benchmark the hybrid approach for image stress calculation is shown in the inset of figure 3. It consists of a curved semi-infinite dislocation represented by three segments in an elastic half space. The lengths of the segments, 0–1, 1–2 and 2–3 are 2 nm, 2 nm and infinite, respectively. Segments 0–1 and 2–3 are parallel to the z-axis, while segment 1–2 is at 30° to the z-axis. The Burgers vector is [111] and all segments are in the $(1\bar{1}0)$ plane. The FEM calculations use a rectangular box with x, y and z dimensions at 30 nm, 30 nm and 12 nm, respectively. Figures 4 (*a*) and (*b*) plot the image force on node 0 and 1, respectively, as a function of the FEM mesh sizes, using both the hybrid and the direct FEM approaches.

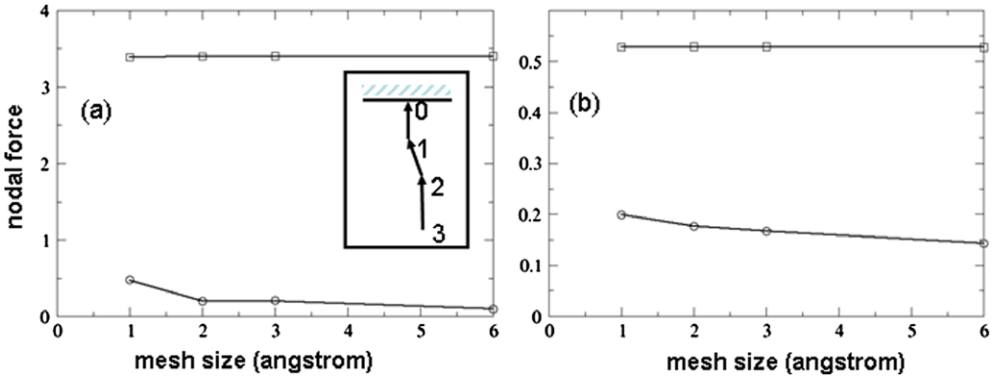

Figure 3. Inset: a three-segment configuration to benchmark the performance of the hybrid method for image stress calculation. The nodal force on nodes 0 and 1 are calculated using image stresses from both the hybrid method and the direct FEM. The magnitude of the nodal force is shown in (*a*) for node 0 and in (*b*) for node 1. The squares are for the hybrid method and the circles are for the direct FEM. The nodal force is in units of μb^2, where μ is the shear modulus.

The most notable feature of these plots is that, the hybrid method based on the 'singular/non-singular decomposition' shows nearly no mesh dependence, whereas the direct FEM approach shows strong mesh dependence. Even when the finest mesh is used (that is still affordable within our computational resources), the results from the direct FEM approach is still far away from the correct, converged values. Analysis shows that the major contribution to the forces on nodes 0 and 1 comes from the image stress of segment 0–1. In the hybrid method, this contribution is computed using the Yoffe analytic solution and is obviously mesh-independent, whereas the direct FEM calculation shows strong mesh dependence due to the difficulty in resolving the singularity. The direct FEM approach significantly underestimates the nodal force because of the insufficient sampling of the singular image stress. The same behaviour was also seen in the ideal case of a straight semi-infinite straight dislocation in an elastic half space, when direct FEM results are compared with the Yoffe analytic solution (Tang *et al* 2003). Although not visible in the figure, the results from the hybrid method also show a very weak dependence on the mesh size. This comes from the non-singular part of the image stresses due to the dislocation segments that are not intersecting the surface. Over the entire range of mesh size considered, the magnitudes of the forces on nodes 0 and 1 only vary by 0.3% and 0.7%, respectively.

3.3. Generalization to multiple free surfaces

So far we have demonstrated the effectiveness of the hybrid method for a curved dislocation in an elastic half space. We have not discussed whether the same method can be generalized to dislocations in elastic bodies with other geometries, such as a finite body with multiple surfaces, as shown in figure 4. Indeed, it may not seem clear whether or not this can be done at all, since the key of the hybrid method is to use the Yoffe analytic solution, which corresponds to an elastic half-space. The hybrid method also requires an auxiliary semi-infinite dislocation segment such as BB′ in figure 4. And the concern is that, if this auxiliary segment intersects another surface, e.g. surface 3, it may exacerbate the situation by introducing yet another singularity. Fortunately, all of these problems can be resolved. In the following, we describe a method that can remove all the singularities from FEM calculations of image stress when the elastic body has multiple surfaces.

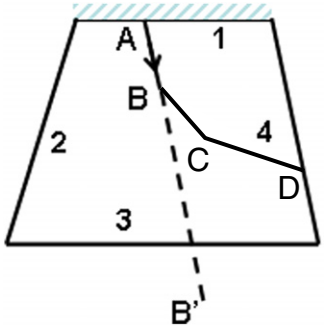

Figure 4. An elastic body with 4 surfaces (1,2,3,4) containing a dislocation line A–B–C–D. When solving for the image stress due to segment A–B, we will make use of the Yoffe solution of a straight semi-infinite dislocation A–B′ in an elastic half space whose surface overlaps with surface 1.

Because the total stress field is the superposition of contributions from all segments, without loss of generality, let us consider the stress field generated by segment A–B, which intersects surface 1 of an elastic body shown in figure 4. Let $\boldsymbol{\sigma}_{\mathrm{AB}}$ be stress field of this segment inside the finite elastic medium, $\boldsymbol{\sigma}^{\infty}_{\mathrm{AB}}$ be the stress field of this segment in an infinite medium, and $\boldsymbol{\sigma}^{\mathrm{img}}_{\mathrm{AB}}$ be the image stress, thus,

$$\boldsymbol{\sigma}_{\mathrm{AB}} = \boldsymbol{\sigma}^{\infty}_{\mathrm{AB}} + \boldsymbol{\sigma}^{\mathrm{img}}_{\mathrm{AB}}. \tag{6}$$

$\boldsymbol{\sigma}^{\mathrm{img}}_{\mathrm{AB}}$ is the stress field inside the elastic medium when its surfaces are subjected to traction forces

$$\boldsymbol{T}_{\mathrm{i}}(\boldsymbol{x}) = -\boldsymbol{\sigma}^{\infty}_{\mathrm{AB}}(\boldsymbol{x}) \cdot \boldsymbol{n}_{\mathrm{i}}, \tag{7}$$

where $\boldsymbol{n}_{\mathrm{i}}$ is the normal vector of surface i. Again, because $\boldsymbol{\sigma}^{\infty}_{\mathrm{AB}}(\boldsymbol{x})$ contains a singularity on surface 1, the convergence of direct FEM approach will be very slow. Let us make use of the Yoffe analytic solution $\boldsymbol{\sigma}^{y-\mathrm{img}}_{\mathrm{AB'}}$, the image stress field of a hypothetical, semi-infinite dislocation AB′, in an elastic half-space, whose surface overlaps with surface 1, as shown in figure 4. Obviously, $\boldsymbol{\sigma}^{y-\mathrm{img}}_{\mathrm{AB'}}$ is a valid solution inside the finite elastic medium, which is a subset of the elastic half-space in which $\boldsymbol{\sigma}^{y-\mathrm{img}}_{\mathrm{AB'}}$ is defined. The total stress contribution from segment A–B can be re-written as

$$\boldsymbol{\sigma}_{\mathrm{AB}} = \boldsymbol{\sigma}^{\infty}_{\mathrm{AB}} + \boldsymbol{\sigma}^{y-\mathrm{img}}_{\mathrm{AB'}} + \boldsymbol{\sigma}^{\mathrm{corr}-\mathrm{img}}_{\mathrm{AB}}. \tag{8}$$

The new image stress $\boldsymbol{\sigma}^{\mathrm{corr}-\mathrm{img}}_{\mathrm{AB}}$ is the stress field inside the elastic medium when all of its surfaces are subjected to traction forces

$$\boldsymbol{T}_{\mathrm{i}}(\boldsymbol{x}) = -(\boldsymbol{\sigma}^{\infty}_{\mathrm{AB}}(\boldsymbol{x}) + \boldsymbol{\sigma}^{y-\mathrm{img}}_{\mathrm{AB'}}(\boldsymbol{x})) \cdot \boldsymbol{n}_{\mathrm{i}}. \tag{9}$$

Since both stress terms in the bracket are non-singular on all surfaces except surface 1, the traction forces in equation (9) are non-singular on those surfaces. Because the Yoffe solution satisfies traction free boundary condition on surface 1, i.e.

$$(\boldsymbol{\sigma}^{\infty}_{\mathrm{AB}} + \boldsymbol{\sigma}^{\infty}_{\mathrm{BB'}} + \boldsymbol{\sigma}^{y-\mathrm{img}}_{\mathrm{AB'}}) \cdot \boldsymbol{n}_1 = 0, \tag{10}$$

on surface 1 equation (9) can be re-written as

$$\boldsymbol{T}_1(\boldsymbol{x}) = -\boldsymbol{\sigma}^{\infty}_{\mathrm{B'B}}(\boldsymbol{x}) \cdot \boldsymbol{n}_1, \tag{11}$$

which is also non-singular, because segment B–B' does not intersect surface 1. Therefore, the new correctional image stress field $\boldsymbol{\sigma}^{\mathrm{corr-img}}$ can be computed using FEM, for an elastic medium subjected to the boundary conditions specified by

$$\begin{cases} \boldsymbol{T}_{\mathrm{i}}(\boldsymbol{x}) = -(\boldsymbol{\sigma}^{\infty}_{\mathrm{AB}}(\boldsymbol{x}) + \boldsymbol{\sigma}^{y-\mathrm{img}}_{\mathrm{AB'}}(\boldsymbol{x})) \cdot \boldsymbol{n}_{\mathrm{i}} \quad i = 2, 3, 4 \\ \boldsymbol{T}_{1}(\boldsymbol{x}) = -\boldsymbol{\sigma}^{\infty}_{\mathrm{B'B}}(\boldsymbol{x}) \cdot \boldsymbol{n}_{1}. \end{cases} \tag{12}$$

Because the traction forces are non-singular on all the surfaces, the FEM calculation is expected to converge very rapidly.

The image stress field of segment BC is simply obtained using the FEM since no singular traction force is involved. The image stress field of segment CD can be obtained similarly as segment AB by applying the Yoffe image solution at surface 4.

In a brief review, this method can be easily generalized to situations where multiple dislocation segments intersect different free surfaces of an elastic medium. In the FEM calculation, the elastic body is subjected to surface traction due to every dislocation segment. Equation (7) is used when a segment does not intersect any surface; equation (12) is used when the segment does intersect a surface. The final image stress is the sum of the FEM result and the Yoffe image solutions of all segments that intersect a surface.

4. Applications

This section discusses two examples of the application of the hybrid method presented above. Both examples are related to dislocation behaviour in a confined space. The first one examines the stress fields produced by a single dislocation threading a thin freestanding film with two free surfaces. The second example is a dynamic simulation of a dislocation half-loop near the surface of an elastic half-space. In both cases, we use the Yoffe solution to obtain accurate image corrections for stress and PK forces on dislocations. The hybrid method allows us to use rather coarse FEM meshes keeping the overall cost of the FEM calculations small compared with the DD part of the problem. To highlight the significance of the image effects, we compare the results with and without the image stress corrections in both examples. In both examples, the major image stress effect is captured by the Yoffe image stress solution alone. We use the mesh size of 0.2 nm to carry out these calculations. The contribution from the correctional image stress by FEM is negligible. One could use a much larger mesh size than 0.2 nm. In fact, we have re-run the example in figure 7 with the Yoffe image stress only, where we have seen the same behaviour.

The first example is a calculation of the stress fields produced by a single screw or edge dislocation in a free standing thin film. The dislocation is straight and threads along the z direction, perpendicular to the top and the bottom free surfaces where traction-free boundary conditions are applied. To gauge the importance of the image stress to dislocation behaviour in thin films, we note that the PK interaction force per unit length between a pair of parallel screw dislocations is $\boldsymbol{f} = \mathrm{b}(\sigma_{\mathrm{yz}}\boldsymbol{i} - \sigma_{\mathrm{xz}}\boldsymbol{j})$, where $\boldsymbol{i}$ and $\boldsymbol{j}$ are the unit vectors along x and y direction, respectively. Figure 5 shows contour plots of the stress component σ_{xz} (in units of shear modulus μ) in the middle plane of the simulation box. The results are similar for σ_{yz}. From (a) to (c), the film thickness changes from 2 to 4 nm to infinity. We can observe that the stress field is confined to a local region whose range is comparable to the film's thickness. This means that the elastic interaction among screw dislocations is significantly modified in the films where it becomes short-ranged. This is because the direction of the Burgers vector is normal to the traction-free surface. A similar observation was made by Eshelby and Stroh (1951). In figure 5, we also plot the stress field of a finite dislocation segment when the image stress is not included, i.e. the canonical solutions only. Although certain size effects can be

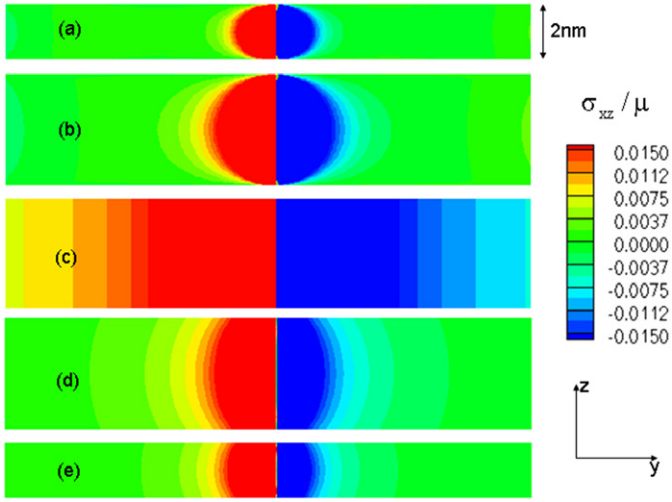

Figure 5. The stress contours computed for a single screw dislocation. The simulation box is 20 nm along the x and y directions. The dislocation lies along the z direction and its Burgers vector is along [001]. The stress contours are computed in the middle plane at $x = 10$ nm. (*a*) and (*b*) show the stress contours in 2 and 4 nm films with the image stress corrections obtained by the hybrid method while (*c*) shows the stress contours due to an infinite screw dislocation. (*d*) and (*e*) show the stress contours of a finite screw segment terminating at the free surfaces in 4 and 2 nm films, but without the image stress correction. Note that the slight asymmetry is due to the fact that the dislocation position is shifted off-centre by 0.05 nm in the positive x and y directions.

observed, the stress distributions are noticeably different from the correct results and violate the traction-free boundary condition at the top and bottom surfaces.

The results for the edge dislocation are qualitatively different. The PK force per unit length between a pair of parallel edge dislocations is $\boldsymbol{f} = \mathrm{b}(\sigma_{\mathrm{xy}}\boldsymbol{i} - \sigma_{\mathrm{xx}}\boldsymbol{j})$. Figure 6 plots the contour plots of σ_{xy} in the middle plane of the simulation box. The results for σ_{xx} are similar. Comparing (*a*) and (*b*) with (c), we see that the effect of the free surface is much smaller than the case in figure 5. The dependence on the film's thickness is also much weaker. This is because, in this case, the dislocation Burgers vector is the same plane as the traction-free surface. Figures 6(*d*) and (*e*) plot the stress distribution when the image correction is not included. In this case, they appear to be overly confined compared with the correct stress distribution.

The second application concerns the stability of a dislocation half-loop beneath a traction-free surface of an elastic half-space. The surface normal is along [001] and coincides with the $z = 0$ plane. The initial condition of the half-loop consists of three straight segments: two edge segments of length 200 b and one screw segment of length 282 b. The Burgers vector is along [110] and parallel to the free surface. Its magnitude is 0.286 nm. A long straight screw dislocation is placed beneath the half-loop at $z = -300$ b with an opposite Burgers vector, so that the half-loop and the screw dislocation should attract each other. The length of the screw dislocation is 707 b and its length is fixed. No cross-slip is allowed so that the segments of both dislocations can move only in the $(1\bar{1}0)$ glide plane. Counteracting the attraction between the half-loop and the long screw dislocation is the image stress from the free surface that pulls the half-loop towards the surface. In these simulations, the dislocation mobility constant M is the same for both screw and edge dislocations (the results are found to be insensitive to the choice of M) and the Peierls stress is $1.5 \times 10^{-4}\,\mu$.

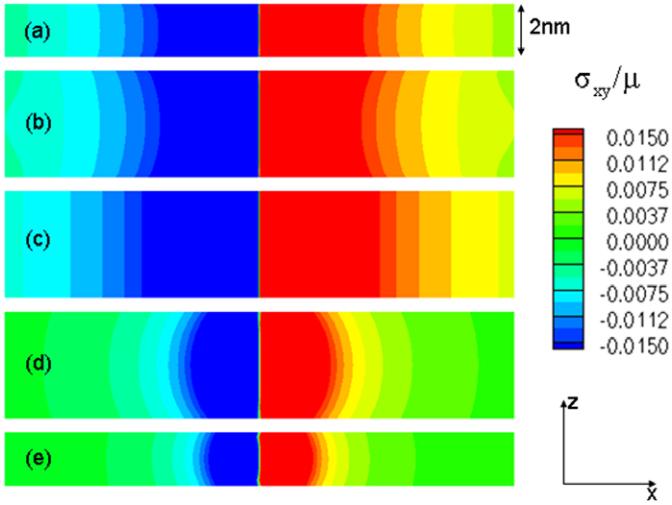

Figure 6. The stress contours computed for a single edge dislocation. The simulation box is 20 nm along the x and y directions. The dislocation lies along the z direction and its Burgers vector is along [100]. The stress contours are computed for the middle plane at $y = 10$ nm. (*a*) and (*b*) show the stress contours in 2 and 4 nm films with image stress corrections computed by the hybrid method while (*c*) shows the stress contour of an infinite edge dislocation. (*d*) and (*e*) show the stress contours of a finite edge segment terminating at the free surfaces in 4 and 2 nm films, but without any image stress correction.

In the first simulation, the image stress field is computed using the hybrid method. The half-loop first turns into a more semi-circular shape, mainly due to line tension effects. Due to the image stress, the half-loop eventually shrinks and disappears at the surface. Snapshots from this simulation are plotted in figure 7(*a*). Next, we repeat the simulation but ignore the image stress field. The behaviour becomes very different. As shown in figure 7(*b*), after some initial relaxation period, the half-loop and the screw dislocation move towards each other and eventually recombines, giving rise to two threading dislocations intersecting the surface. These two simulations illustrate the importance of image stress corrections on the fate of a dislocation half-loop near the surface, which can be important for the nucleation of threading dislocations for stress relaxation in thin films.

5. Summary

In this paper, we presented a new method for computing the image stresses produced by an arbitrary dislocation arrangement in a finite isotropic elastic body with one or more traction-free surfaces. The method is based on a special treatment of the singular part of the image stress for dislocation segments intersecting traction-free surfaces. The hybrid method achieves a high accuracy and computational efficiency by dispensing with the need for excessive mesh refinement near the termination points. At present, our approach relies on the standard framework of the singular continuum theory of dislocations. Further development is underway to extend this approach to a non-singular version of the continuum theory (Cai *et al* 2005).

The examples given in this paper demonstrate the importance of the image stress in confined spaces. In a freestanding thin film, when the Burgers vector is normal to the surface, the image stress is found to significantly alter the interaction range between two dislocations. A much weaker effect is found when the Burgers vector is in the plane parallel to the free

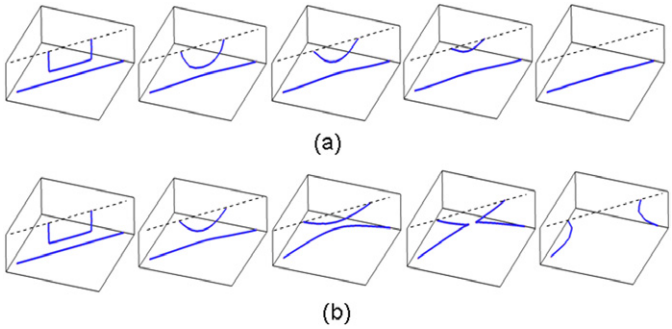

Figure 7. Snapshots from DD simulations of a dislocation half-loop and an initially straight dislocation beneath a free surface. The two ends of the straight dislocation are fixed in space. Time proceeds from left to right. The dashed line indicates where the free surface is. (*a*) When the image stress is fully accounted for, the half-loop eventually disappears at the free surface. (*b*) When the image stress is ignored, the half-loop eventually recombines with the dislocation below, leaving two threading dislocations intersecting the free surface.

surface. In the case of a dislocation half-loop beneath the surface of an elastic half-space, the image stress is found to be important in the fate of the half-loop. Further calculations are underway to study the effect of image stresses on dislocation behaviour in small systems with more complex geometries. We expect that this method will be useful for the study of size effects of crystal plasticity at small scales.

Acknowledgments

We thank Drs P Hazzledine, R Rudd, and J Moriarty for fruitful discussions. This work is performed under the auspices of the US Department of Energy (DOE) by the University of California, Lawrence Livermore National Laboratory under Contract No. W-745-Eng-48.

References

Brown L M 1964 The self-stress of dislocations and the shape of extended nodes *Phil. Mag.* **10** 441

Bulatov V V, Cai W, Fier J, Hiratani M, Pierce T, Tang M, Rhee M, Yates K and Arsenlis A 2004 Scalable line dynamics of ParaDiS *SuperComputing* p 19 online at http://www.sc-conference.org/sc2004/schedule/pdfs/pap206.pdf

Bulatov V V, Tang M and Zbib H M 2001 Dislocation plasticity from dislocation dynamics *MRS Bull.* **26** 191

Cai W 2001 Atomistic and mesoscale modeling of dislocation mobility *PhD Thesis* Massachusetts Institute of Technology

Cai W, Arsenlis A, Weinberger C R and Bulatov V V 2005 A non-singular continuum theory of dislocations *J. Mech. Phys. Solids* **54** 561

Cai W and Bulatov V V 2004 Mobility laws in dislocation dynamics simulations *Mater. Sci. Eng.* A **387–389** 277

Cai W, Bulatov V V, Chang J, Li J and Yip S 2004a Dislocation core effects on mobility *Dislocations in Solids* vol 12 ed F R N Nabarro and J P Hirth (Amsterdam: Elsevier) p1

Cai W, Bulatov V V, Pierce T G, Hiratani M, Rhee M, Bartelt M and Tang M 2004b Massively-parallel dislocation dynamics simulations *Solid Mechanics and Its Applications* vol 115 ed H Kitagawa and Y Shibutani (Dorchet: Kluwer) p 1

Devincre B 1995 Three dimensional stress field expressions for straight dislocation segments *Solid State. Commun.* **93** 875

Devincre B 1996 Meso-scale simulation of the dislocation dynamics *Computer Simulation in Materials Science* vol 308 ed H O Kirchner *et al* NATO ASI Series E (Dordrecht: Kluwer) p 309

Eshelby J D 1979 Boundary problems *Dislocations in Solids* vol 1 ed F R N Nabarro (New York: North-Holland) p 167

Eshelby J D and Stroh A N 1951 Dislocations in thin plates *Phil. Mag.* **42** 1401
Fivel M C, Gosling T J and Canova G R 1996 Implementing image stresses in a 3D dislocation simulation *Modelling Simul. Mater. Sci. Eng.* **4** 581
Gavazza S D and Barnett D M 1976 The self-force on a planar dislocation loop in an anisotropic linear-elastic medium *J. Mech. Phys. Solids* **24** 171
Ghoniem N M, Tong S–H and Sun L Z 2000 Parametric dislocation dynamics: A thermodynamics-based approach to investigations of mesoscopic plastic deformation. *Phys. Rev.* B **61** 913
Hazzledine P M and Shaibani S J 1982 The behaviour of dislocations near a free surface *ICSMA* ed R C Gifkins (Oxford: Pergamon) p 45
Hirth J P and Lothe J 1982 *Theory of Dislocations* 2nd edn (New York: Wiley)
Honda K 1979 Dislocation walls consisting of double arrays in white tin single crystals *Japan. J. Appl. Phys.* **18** 215
Hughes T J R 2000 *The Finite Element Method: Linear Static and Dynamic Finite Element Analysis* (New York: Dover)
Khraishi T A and Zbib H M 2002 Free-surface effects in 3D dislocation dynamics: formulation and modeling *J. Eng. Mater. Tech.* **124** 342
Kubin L P and Canova G R 1992 The modelling of dislocation patterns *Scr. Metall. Mater.* **27** 957
Kukta R V 1998 *PhD Thesis* Brown University
Lemchand C, Devincre B and Kubin L P 2001 Homogenization method for a discrete-continuum simulation of dislocation dynamics *J. Mech. Phys. Solids* **49** 1969
Liu X H, Ross F M and Schwarz K W 2000 dislocated epitaxial islands *Phys. Rev. Lett.* **85** 4088
Liu X H and Schwarz K W 2005 Modelling of dislocations intersecting a free surface, *Modelling Simul. Mater. Sci. Eng.* **13** 1233
Lothe J 1992 Dislocations in continuous elastic media *Elastic Strain Fields And Dislocation Mobility* ed V L Indenbom and J Lothe (Amsterdam: North-Holland) p 175
Martinez R and Ghoniem N M 2002 The Influence of crystal surfaces on dislocation interactions in mesoscopic plasticity: a combined dislocation dynamics- finite element approach *J. Comp. Meth. Eng. Sci.* **3** 229
Shaibani S J and Hazzledine P M 1981 The displacement and stress fields of a general dislocation close to a free surface of an isotropic solid *Phil. Mag.* **44** 657
Schwarz K W 1999 Simulation of dislocations on the mesoscopic scale. I. Methods and examples *J. Appl. Phys.* **85** 108
Smith I M and Griffiths D V 1998 *Programming the Finite Element Method* 3rd edn (NewYork: Wiley)
Tang M, Kubin L P and Canova G R 1998 Dislocation mobility and the mechanical response of B.C.C. single crystals: a mesoscopic approach *Acta Mater.* **46** 3221
Tang M, Xu G, Cai W and Bulatov V V 2003 Dislocation image stresses at free surfaces by the finite element method *Thin Film Stresses and Mechanical Properties* ed S G Corcoran *et al* (Warrendale, PA: Materials Research Society) **795** U2.4
Van der Geissen E and Needleman A 1995 Discrete dislocation plasticity: a simple planar model *Modelling Simul. Mater. Sci. Eng.* **3** 689
Wang Z, McCabe R J, Ghoniem N M, LeSar R, Misra A and Mitchell T E 2004 Dislocation motion in thin Cu foils: comparison between computer simulations and experiment *Acta Mater.* **52** 1535
Weygand D, Friedman L H, Van der Geissen E and Needleman A 2002 Aspects of boundary-value problem solutions with three-dimensional dislocation dynamics *Modelling Simul. Mater. Sci. Eng.* **10** 437
Yan L, Khraishi T A, Shen Y L, and Horstemeyer M F 2004 A distributed dislocation method for treating free-surface image stresses in three dimensional dislocation dynamics simulations *Modelling Simul. Mater. Sci. Eng.* **12** 289
Yasin H, Zbib H M and Khaleel M A 2001 Size and boundary effects in discrete dislocation dynamics: coupling with continuum finite element *Mater. Sci. Eng.* A **309–310** 294
Yoffe E H 1961 A dislocation at a free surface *Phil. Mag.* **6** 1147
Zbib H M, Rhee M and Hirth J P 1998 On plastic deformation and the dynamcis of 3D dislocations *Int. J. Mech. Sci.* **40** 113